Fluid flow in a helical vessel in presence of a stenosis

Luigino Zovatto · Gianni Pedrizzetti

Abstract Large arteries are not straight and rather present curvature and torsion. The present study analyzed fluid flow in a helical vessel without and with a stenosis in comparison with an analogous rectilinear vessel. The analysis is performed by three-dimensional numerical simulation of the Navier–Stokes equations under steady conditions considering stenosis as an axially symmetric reduction of vessel lumen. Results show that the double curvature gives rise to persistent secondary motion which combines with the vorticity separated behind the constriction to develop a complex three-dimensional vorticity structure. The curved streamlines and the three-dimensional vortex wake result in a increase of energetic losses in helical vessels. However, the same symmetry break due to the double curvature improves the capacity of self-cleaning and allows a more rapid wash-out of the flowing blood.

Keywords Arterial flow · Helical vessel · Separation

L. Zovatto (✉) · G. Pedrizzetti
Dipartimento Ingegneria e Architettura, Università degli Studi di Trieste, Trieste, Italy
e-mail: zovatto@dicar.units.it

1 Introduction

This study is dedicated to analysing the flow field inside a helical vessel in the presence of a reduction of its lumen (i.e stenosis) and comparing it with the analogous flow that establishes in a rectilinear vessel. The study takes its cue from the initial intuition of Caro [1] and follows later observations made in vivo and in biomedical models. These have shown that the presence of a no-planar curvature in a blood vessel (e.g aorta, carotid) induces secondary motions which avoid the development of stagnation in the regions downstream the separation of the boundary layer [2]. This fact presents important clinical implications, like the reduction of the risk of atherosclerosis, such that recent studies suggested to introduce diagnostic indexes of vascular risk based on flow helicity [3].

The hydrodynamic analysis first characterizes the presence of secondary circulation which develops in the helical vessel. The longitudinal vorticity corresponding to secondary circulations is expected to combine with the transversal circulation due to boundary layer separation downstream the constriction. This vorticity interaction develops a complex three-dimensional wake structure which differs from normal recirculation regions, possibly presenting open streamlines and limited areas of stagnation.

The vorticity analysis is thus integrated, in the second part of the work, by investigating the ability of blood wash-out using a transport model for a passive

scalar which initially fills the entire lumen. The results are evaluated in terms of concentration of the solute and residence time distribution (RTD) to asses the comparative wash-out properties of helical and rectilinear vessels, with and without stenosis.

2 Model formulation

2.1 Fundamentals

This study considers the motion of an incompressible fluid inside a helical vessel. Geometric parameters are taken from analogy with large arteries with the radius and the pitch of the helix axis $\rho = 1.5D$ and $p = 2\pi D$, respectively, being D the vessel diameter. Only one pitch length of the vessel is considered in compliance with the finite length of an artery tract. Then the stenosis is considered as axially symmetric with 50 % reduction of lumen area and a predefined smooth longitudinal shape. The present fluid dynamics investigation was performed numerically under steady state conditions. The Navier–Stokes equations governing the phenomena are solved for a Reynolds' number, $Re = VD/v$, equal to 1000, a value compatible with flows in the medium and large size arteries, being the average velocity V and v the kinematic viscosity.

In what follows, the diameter D and the velocity V are used as reference units for the dimensionless formulation.

2.2 Helical geometry of the vessel axis

A helix is a three-dimensional space curve $\overrightarrow{x_h}$ described by the parametric equations

$$x_h = \rho cos(t), \quad y_h = \rho sin(t), \quad z_h = ct; \qquad (1)$$

where $c = \frac{p}{2\pi}$ and t, $0 < t < 2\pi$, is the parametric coordinate along the curve.

The helix curvature and torsion are given by $\kappa = \frac{\rho}{\rho^2+c^2}$ and $\tau = \frac{c}{\rho^2+c^2}$, respectively. Then, the Frenet triad of tangent, normal and binormal unit vectors are then defined by

$$\overrightarrow{T} = \frac{d\overrightarrow{x_h}}{ds}, \quad \overrightarrow{N} = \frac{1}{\kappa}\frac{d\overrightarrow{T}}{ds}, \quad \overrightarrow{B} = \overrightarrow{T} \times \overrightarrow{N}; \qquad (2)$$

where s is the helix arc length which increases linearly with the parametric coordinate t

$$s = \int_0^t \sqrt{\left(\frac{dx_h}{dt}\right)^2 + \left(\frac{dy_h}{dt}\right)^2 + \left(\frac{dz_h}{dt}\right)^2}\, dt = \sqrt{\rho^2 + c^2}\,t. \tag{3}$$

2.3 Coordinate system

In this study we consider helical coordinate system first proposed by Wang and Caro [4]. Such an approach considers planar sections perpendicular to the helix axis $\overrightarrow{x_h}(s)$ (1), and introduces a coordinate system (s, r, θ) such that a generic position vector in Cartesian coordinates $\overrightarrow{x}$ is given by

$$\overrightarrow{x}(s, r, \theta) = \overrightarrow{x_h}(s) + rcos(\theta)\overrightarrow{N}(s) + rsin(\theta)\overrightarrow{B}(s). \tag{4}$$

Taking the dot product of the incremental change of equation (4)

$$d\overrightarrow{x} \cdot d\overrightarrow{x} = (dr)^2 + R_p^2(d\theta)^2 + [(1 - k\tau cos(\theta)^2 R_p^2]ds^2 + 2\tau R_p^2 dsd\theta \tag{5}$$

produces the mixed term $2\tau R_p^2 dsd\theta$ which highlights that such coordinate system is non-orthogonal.

A following paper [5], showed that it is sufficient to replace θ in (4) with $\theta + \tau s$, to end up with an orthogonal coordinate system. However, literature [6, 7] showed that the velocity field in the two coordinate systems are related by a simple transformation. In the same work, it was also demonstrated that the effect of torsion and secondary circulation were more easily identified within the non-orthogonal system (4). While the orthogonal system is best suited for analytical studies, the (slightly) non-orthogonal is more practical in the finite element numerical method employed here.

2.4 Helical vessel

The equation for a point the helical vessel is then described by

$$
\begin{aligned}
x &= ct - \kappa r\, sin(\theta), \\
y &= \rho\,cos(t) + r\,(cos(\theta)\cos(t) - \tau sin(\theta)sin(t)), \\
z &= \rho\,sin(t) + r\,(cos(\theta)\sin(t) + \tau sin(\theta)cos(t));
\end{aligned}
\tag{6}
$$

where the three-dimensional parametric coordinates are $0 \le t \le 2\pi$, along the vessel axis, $0 \le \theta \le 2\pi$,

azimuthal in a cross section, and $0 \leq r \leq R(t)$, radial. Here $R(t)$ is the radius of the vessel whose value outside the stenosis is $R = \frac{1}{2}$. The vessel radius at the stenosis was describes as Gaussian hill with a 50 % maximal reduction of the cross section in the mid-length, $t = \pi$ of the vessel. In formulae

$$R(t) = \frac{1}{2} - \frac{(2 - \sqrt{(2)})}{4} e^{-\frac{13}{8} \frac{(\pi - t)^2}{3 - \sqrt{8}}}; \qquad (7)$$

The helical vessel used in the analysis is shown in Fig. 1.

The straight vessel used for comparison is described in terms of the same parametric coordinates by the simple equation

$$\begin{aligned} x &= c_0\, t, \\ y &= r\cos(\theta), \\ z &= r\sin(\theta); \end{aligned} \qquad (8)$$

where c_0 is a constant factor, equal to $\sqrt{\rho^2 + c^2}$ to ensure a same finite length of the rectilinear and helical vessels.
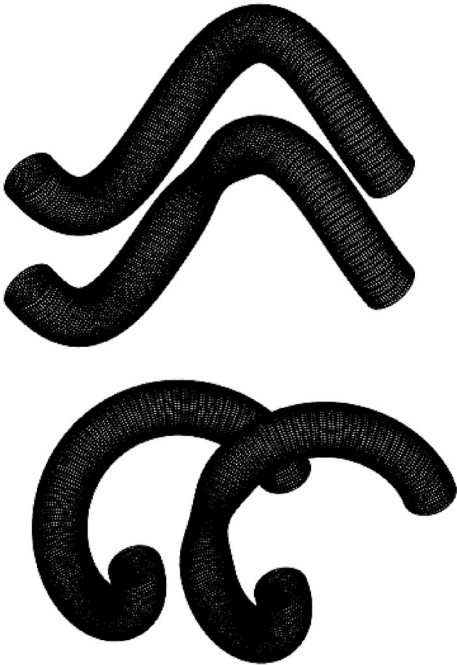

Fig. 1 Helical vessel with constant section and with stenosis. Parametric coordinates are $0 \leq t \leq 2\pi$, along the vessel axis, $0 \leq \theta \leq 2\pi$, azimuthal in a cross section, and $0 \leq r \leq R(t)$, radial; while helical radius is $\rho = 1.5$

3 Numerical method

The analysis was performed numerically by means of a finite element method where the space domain is discretized with tetrahedral elements. For maximum simplicity, the variables have been assumed to change linearly within every element. Momentum and mass balance equation are written dimensionless form

$$\frac{\partial \overrightarrow{u}}{\partial t} + \overrightarrow{u}\nabla \overrightarrow{u} = \nabla P + \frac{1}{Re}\Delta \overrightarrow{u} \qquad (9)$$

$$\nabla \cdot \overrightarrow{u} = 0 \qquad (10)$$

where $\overrightarrow{u}$ represent the velocity vector field, P the pressure field and Re is Reynolds number. Differential equations 9 and 10 are rewritten on the finite element mesh using a Galerkin residual procedure [8], resulting in a second-order accuracy in space.

Boundary conditions are given at the inlet by prescribing the Poiseuille profile, corresponding to Dirichlet conditions for all velocity components, and at the outlet by imposing null total stress. No-slip condition is enforced on all the rigid walls.

Steady-state solution is achieved by time-marching the momentum equation with second-order fully implicit and variable time step. Every simulation was impulsively started from rest and marched until convergence, in all cases the steady regimes were reached within about 20 time units. The number of nodes employed for the discretization ranged was about 5×10^6 (20×10^6 elements) with a grid refinement near the walls and in the stenosis region, eventually the typical size of smaller elements is about 1×10^{-3}.

3.1 Validation test

First, an extensive grid refinement analysis was performed to verify the adequacy of the discrete representation of domain for all vessels, with particular attention to the helical vessel with stenosis. The grid was refined by cutback of two times the maximum and minimum size parameters of the mesh generator; in this way the number of tetrahedral elements is approximately doubled. Figure 2 shows the variation of the normal component of velocity in the helical vessel axis in the output section versus the average size of the element; no significant physical difference can be detected.
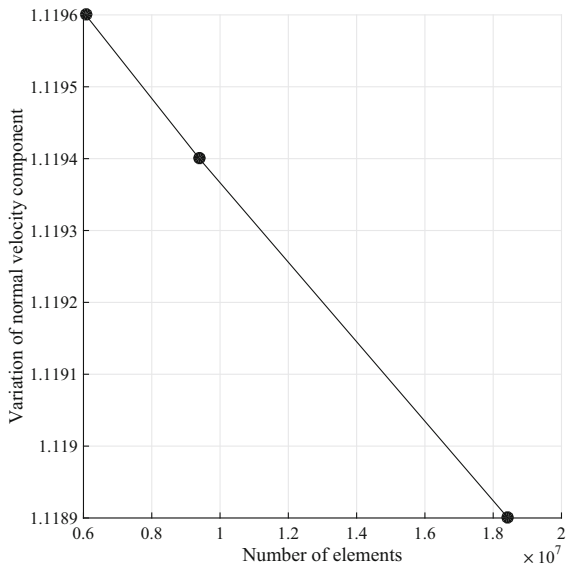
3

Fig. 2 Variation of the normal component of velocity in the helical vessel axis in the output section, versus the number of the elements
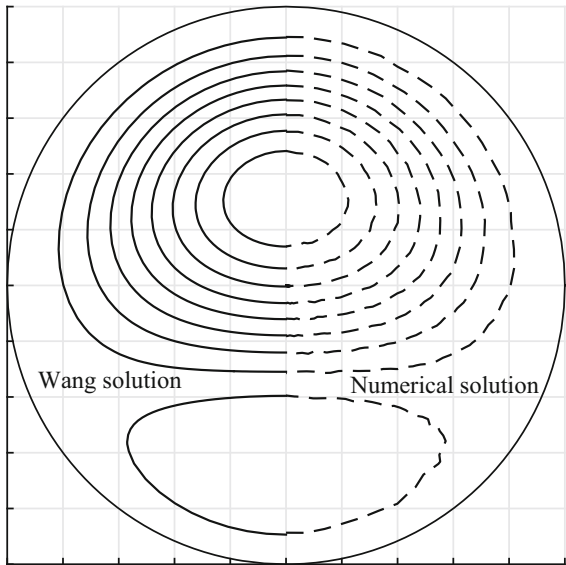

Fig. 3 Secondary flow: solution proposed from Wang and numerical results, when the parameter $\lambda = \frac{c}{R}\frac{1}{Re}$ is equal to 0.01

Secondly, we considered the analytic solutions obtained in [4] by means of pertubative method for the flow in an helical vessel of constant cross-section. The comparison is shown in Fig. 3 and presented an excellent agreement.

4 Results

4.1 Secondary circulation

In the rectilinear vessel, as previously shown in literature (see for example [9]), secondary circulations do not develop. The boundary layer detaches from the wall after the stenosis and develops a primary circulatory region which remains attached to the wall, Fig. 4. At this Reynolds number the separated region is stationary and gives rise to a stagnation zone bounded by a limiting streamline.

The motion field in the helical vessel is characterized by a pair of secondary circulation cells regardless of the presence of stenosis. The presence of such transversal vortices, whose total circulation is zero, can be detected by the analysis of the streamlines in a cross-section. The secondary flow field also induces a shift of the axis of the vortices as shown in Fig. 5. The rotation of the vortex center does not have the same pitch of the helical vessel since the length is not sufficient to develop a synchronous rotation. The presence of stenosis affects marginally the secondary flow structure: secondary vortices are almost identical upstream the stenosis, Fig. 6; the center of the main vortex core remains in the same position even inside the stenosis, Fig. 7, although the counter-rotating vortex is less evident because pressed to the wall by to the flow acceleration; a difference in the main secondary circulation is found behind the stenosis where it combines with the separating boundary layer, Fig. 8. It should be remarked that Fig. 5 is drawn in the global coordinate system that allows an immediate evaluation of the axial shifting of the vortices, whereas Figs. 6, 7 and 8 are drawn with respect to the local coordinate system, the Frenet frame, given by appropriate triplet of unit vectors Eq. 2; in Figs. 6, 7 and 8 the red streamlines correspond to the kernel of the principal vortex, while the green streamlines are the kernel of the counter-rotating vortex.
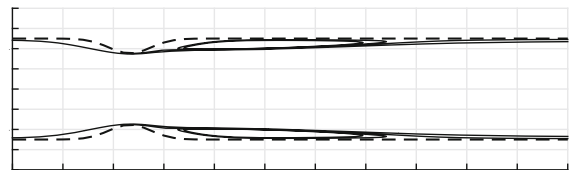

Fig. 4 Streamlines near to the wall after the stenosis for the rectilinear vessel, *dotted lines* represent the walls
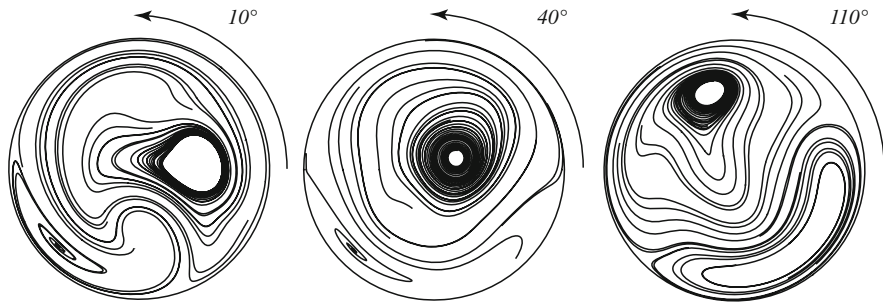
Fig. 5 The secondary flow field induces a shift of the vortex. Secondary streamlines, in the global coordinates frame, are represented in sections for $t = \frac{\pi}{2}$, $t = \pi$, $t = 3\frac{\pi}{2}$. External to each picture, the rotation with respect the axis of the main vortex is indicated
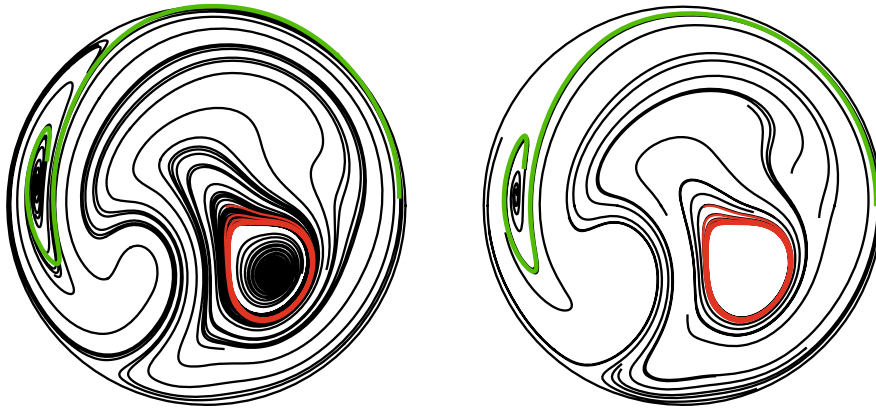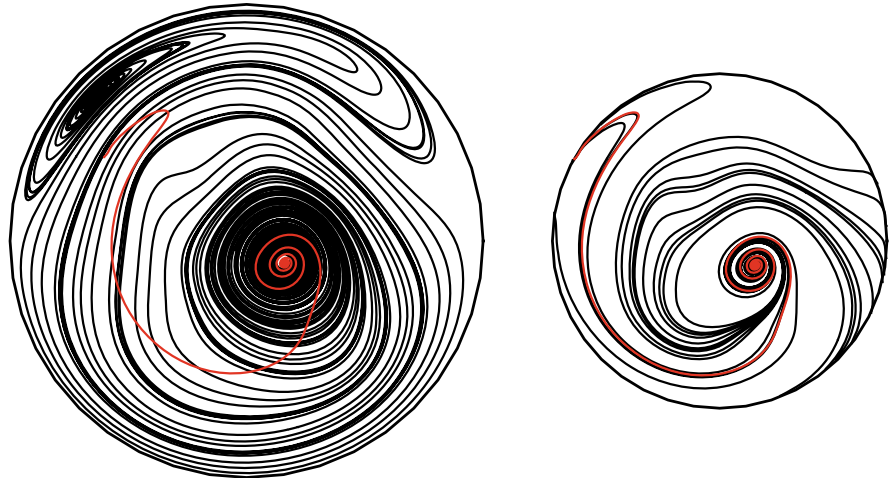

Fig. 6 Streamlines for helical vessel (*left side*) and helical vessel with stenosis (*right side*) upstream the stenosis, $t = \frac{\pi}{2}$, drawn in the local (Frenet triplet) coordinate frame. The position of the main vortex is not altered by the presence of the downstream stenosis. *Red* and *green* streamlines represent the kernel of the principal (*red*) and counter-rotating (*green*) circulations. (Color figure online)

Fig. 7 Streamlines for helical vessel (*left side*) and helical vessel with stenosis (*right side*) at the center of the stenosis, $t = \pi$, drawn in the local (Frenet triplet) coordinate frame. The center of the main vortex is about in the same position although the counter-rotating circulation is less evident due to flow acceleration at the stenosis. *Red* streamlines represent the kernel of the principal circulations. (Color figure online)
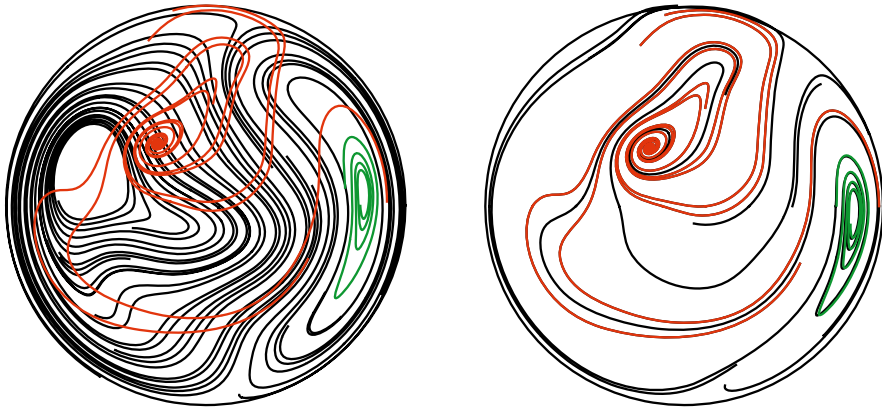
Fig. 8 Streamlines for helical vessel (*left side*) and helical vessel with stenosis (*right side*) downstream the stenosis, $t = \frac{3}{2}\pi$, drawn in the local (Frenet triplet) coordinate frame. The main secondary circulation vortex is some altered by the stenosis, whereas the counter-rotating circulation is about unaffected. *Red* and *green* streamlines represent the kernel of the principal (*red*) and counter-rotating (*green*) circulations. (Color figure online)

Fig. 9 3D vortex structure downstream of the stenosis of the rectilinear vessel
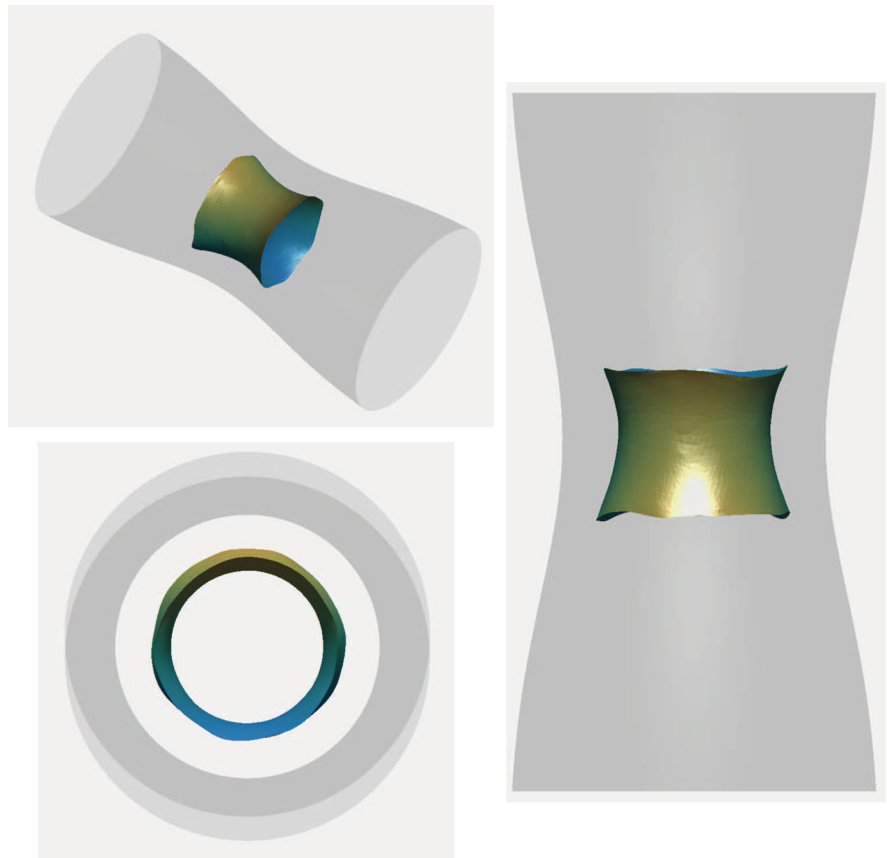
4.2 Three-dimensional vortex structure

The three-dimensional (3D) structure of the vortex downstream the stenosis has been analyzed using the λ_2 method [10, 11]. The vortex structure in the rectilinear vessel is shown in Fig. 9. It presents an axisymmetric shape, given by a vortex layer that generates at the stenosis and extends downstream. It
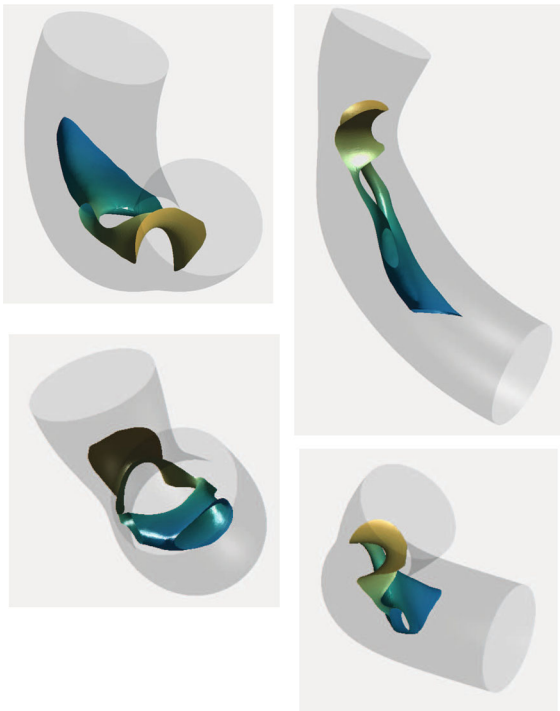
6

Fig. 10 Vortex structure downstream of the stenosis of the helical vessel

Table 1 Pressure losses measured in the vessels

	Rectilinear	Helical
Total loss without stenosis	1.00	2.88
Total loss with in stenosis	2.75	5.66
Local loss imputable to stenosis	1.75	2.78

corresponds to a closed recirculation region downstream the stenosis.

The picture is substantially different in the helical vessel because the helical geometry breaks the axial symmetry of the stenosis thus giving rise to a 3D vortex structure. The boundary layer separating from the axisymmetric stenosis does not give rise to circular vortex lines because the strength of the separating vorticity is modulated by the non-axisymmetric velocity that develops near the wall; concurrently, this azimuthal vorticity combines with the longitudinal vorticity corresponding to the secondary circulation describe above. Eventually, as shown in Fig. 10, the separated vorticity develops streamwise counter-rotating vorticity filaments.

4.3 Pressure losses

Following the markedly different flow geometry, the presence of the streamwise vortices in the helical vessel alters dramatically the shear stresses that develop at the wall. This is quantified by the pressure losses in the entire vessel that are reported in Table 1,

the corresponding pressure profiles along the vessel are reported in Fig. 11. In absence of stenosis, the helical geometry causes an increase of the wall shear stresses and of energetic dissipation because the non-rectilinear geometry deviates the flow and curves the streamlines. In both vessels, in presence of stenosis the pressure profile shows the additional localized loss due to the increased friction at the constriction. However, the rectilinear duct presents the well-known pressure recovery phenomenon behind the stenosis, which is due to the recirculation cell in the enlarged section. Differently enough, the recovery is absent in helical vessel because the wake does not present backward motion and the net loss at the stenosis is irremediably lost and not recovered afterward.

Therefore, by an energetic perspective, the helical vessel gives an increased energy loss that is further amplified in presence of a stenosis, and performs worse than a corresponding rectilinear vessel.

4.4 Residence time distribution

The flow structure in the rectilinear and helical geometry are also different in kinematic terms, because the former presents a closed recirculation region, with closed streamlines, while the wake in the latter is an open flow structure with streamlines entering and exiting from it. This phenomenon is expected to give rise to different performances in terms of ability for wash-out which is analyzed here in terms of residence time of blood elements.

The concept of residence time distribution (RTD) was developed long time ago in reactive chemical engineering, e.g. [12], and is also useful to quantify the the presence of blood stagnation regions which can increase the risk of cloth formation in cardiac flows [13].

The analysis of RTD can be obtained by the solution of the convection-diffusion equation for studying the wash-out of arbitrary passive scalar

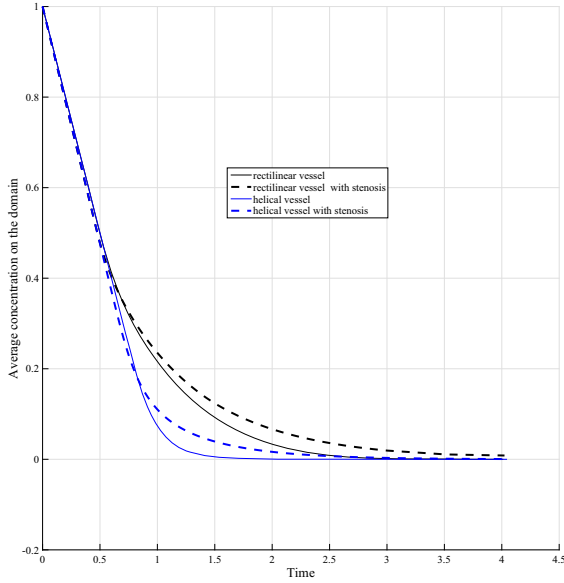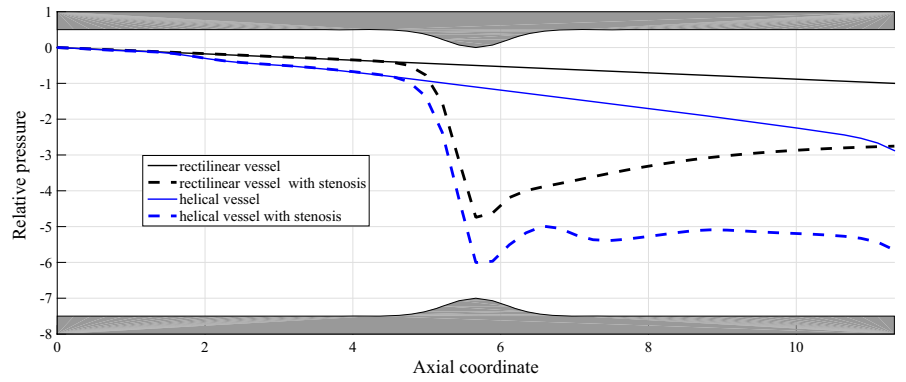**Fig. 11** Relative pressure profile along the vessels

Fig. 12 Average concentration in the domain versus time. Time unit during wash-out is scaled by the time required by an particle to travel the entire vessel with the average velocity

Fig. 13 Section's average concentration versus the axis, at wash-out scaled time equal to 1

$c(\overrightarrow{x}, t)$ that initially fills the entire vessel (initial blood volume)

$$\frac{\partial c}{\partial t} + \overrightarrow{u} \nabla c = \frac{1}{Re} \Delta c \tag{11}$$

with initial condition $c(\overrightarrow{x}, 0) = 1$. Inlet boundary conditions is $c(0, t) = 0$, outlet condition is $\frac{\partial c(0,t)}{\partial n} = 0$, and no-flux condition is enforced on all the rigid walls. The same diffusive coefficient of the momentum Eq. (9), i.e. Re^{-1}, is used here because the scalar is the blood itself. Figure 12 reports the average concentration in the entire domain during time. For
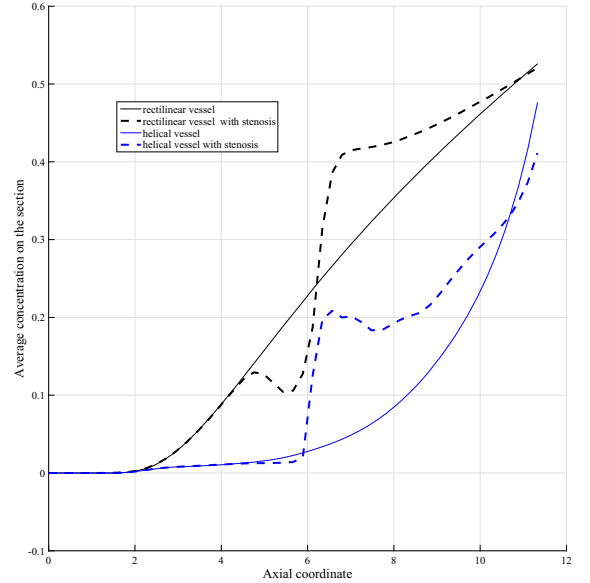
convenience, time is here scaled by a reference wash-out period: the time required by a particle to travel the entire vessel with the average velocity. It shows that the wash-out is slower in the rectilinear vessel which presents a larger concentration (initial blood volume) for most of the time. Indeed, blood exhibits a high residence time close to the walls and gets trapped for a longer time in the circulation cell behind the stenosis. Residence times are highly reduced in the helical vessel even in presence of the stenosis because secondary motion improves the wash-out of the fluid close to the wall and the wake is an open structure that does not trap fluid elements.
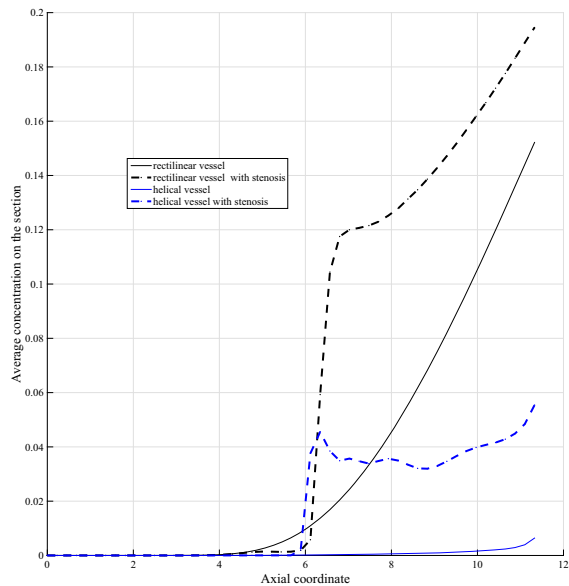
Fig. 14 Section's average concentration versus the axis, at wash-out scaled time equal to 2

This fact is further demonstrated by looking at the distribution of concentration along the vessel at two intermediate instants in Figs. 13 and 14 after 1 and 2 wash-out periods, respectively. In absence of stenosis, the slow moving blood near the wall is washed-out more rapidly in the helical geometry by the combination of longitudinal and secondary motion, it must be emphasized that the reference wash-out period is the same among all the studied cases for Figs. 12, 13 and 14. Furthermore, the open wake behind the stenosis avoids the phenomenon of fluid trapping found in the rectilinear vessel and reduces the residence time in the wake region.

Therefore, the helical geometry allows a more rapid wash-out of flowing blood; this is in agreement with previous in vivo observations for which a blood vessel with double curvature reduces the deposit of biological material [1].

5 Conclusion

The present steady flow analysis highlights important differences about blood motion in doubly curved vessels with respect to rectilinear ones.

The double curvature gives rise to persistent secondary motion that is only moderately influenced by the presence of a stenosis. This secondary motion corresponds to longitudinal vorticity components which breaks the symmetry of rectilinear vessels. This streamwise vorticity interacts with the transversal vorticity that separates from the stenotic constriction producing an open three-dimensional vorticity structure.

On one side, the curved streamlines and the more complex vortex wake produce an increase of energy losses in helical vessels. On the other side, the same increase in complexity and symmetry break avoid the development of stagnation regions and improve the capacity of self-cleaning.

References

1. Caro CG, Doorly DJ, Tarnawski M, Scott KT, Long Q, Dumouling CL (1996) Non-planar curvature and branching of arteries and non-planar-type flow. Proc R Soc A 452:185–197
2. Coppola G, Caro CG (2009) Arterial geometry, flow pattern, wall shear and mass transport: potential physiological significance. J R Soc Interface 6:519–528
3. Gallo D, Steinman DA, Bijari PB, Morbiducci U (2012) Helical flow in carotid bifurcation as surrogate marker of exposure to disturbed shear. J Biomech 45:2398–2404
4. Wang CY, Caro CG (1981) On the low-Reynolds-number flow in a helical pipe. J Fluid Mech 108:185–194
5. Germano M (1981) On the effect of torsion on a helical pipe flow. J Fluid Mech 125:1–8
6. Tuttle ER (1990) Laminar flow in twisted pipes. J Fluid Mech 219:545–570
7. Cookson AN, Doorly DJ, Sherwin SJ (2010) Using coordinate transformation of Navier–Stokes equations to solve flow in multiple helical geometries. J Comput Appl Math 234:2069–2079
8. Zienkiewicz OC (1977) The finite elements method, 4th edn. McGraw-Hill, New York City
9. Pedrizzetti G (1996) Unsteady tube flow over an expansion. J Fluid Mech 310:89–111
10. Jeong J, Hussain F (1995) On the identification of a vortex. J Fluid Mech 285:69–94
11. Domenichini F, Pedrizzetti G, Baccani B (2005) Three-dimensional filling flow into a model left ventricle. J Fluid Mech 539:179–198
12. Pareek VK, Yap Z, Brungs MP (2001) Adesina, Particle residence time distribution (RTD) in three-phase annular bubble column reactor. Chem Eng Sci 56:6063–6071
13. Mangual JO, Domenichini F, Pedrizzetti G (2012) Describing the highly three dimensional right ventricle flow. Ann Biomed Eng 40:1790–1801